A REVIEW ON ANODIC ELECTRICAL BREAKDOWN PHENOMENA IN DIELECTRIC MATERIALS

Kulikov V.
Doctor of Phys.- Math. Sciences. Professor
Tomsk Agricultural Institute – a Branch of the Novosibirsk State Agrarian University, Tomsk, Russia
https://doi.org/10.5281/zenodo.10817074

Abstract
Qualitative and quantitative interpretation of the laws governing the formation of the anodic channel of electrical breakdown in various materials was made within the framework of the mechanism of generation of free electrons through interatomic Auger transitions in the valence band of the dielectric.

Keywords: electrical breakdown in dielectrics, impulse breakdown

Introduction

Polymer materials, silicon dioxide, aluminum oxide, boron nitride are widely used in various electrical devices as insulating coatings and dielectric layers [1-3]. Transformer oil, as the basis for insulation and cooling, is used in high-voltage transformers and switches [4, 5]. Reversible electrical breakdown in semiconductor compounds of the A^2B^6 type is in demand in the development of pulsed streamer lasers [6, 7]. The high dielectric constant and high pulsed electrical strength of water (~ 0.5 MV/cm) make it possible to use water insulation in the forming line of pulsed high-current accelerators of charged particles in the megavolt range [8]. Historically, alkali halide crystals (AHC) are the basis for studying the physical processes of electrical breakdown [9-11].

One of the most important tasks during the development of such facilities is to increase the reliability of insulation, in particular, to prevent the breakdown of dielectric units and media under exposure of extreme electric fields. On the other hand, there are devices where breakdown is the basis of their functioning, for example, solid dischargers [12], electric pulse technologies for the destruction of rocks, concrete, and building materials [13]. Both the problems of breakdown prevention and the problems of insulation coordination and control of the breakdown process require a deep understanding of the fundamental physical mechanisms of the breakdown process in various substances — crystalline, ceramic, liquid.

A large amount of experimental material shows fairly general properties of breakdown in condensed matter (see, for example, [9-11, 14-18]). The breakdown usually occurs from a positively charged electrode (anode breakdown). Anodic breakdown is characterized by a high pre-breakdown current density (~10^4 A/cm^2). The crystallographic orientation of the breakdown channels is observed. The speed of the channel is quite high and amounts to 10^7 - 10^8 cm/s, the channel diameter is in the range of ~ 2-20 μm.

The electron avalanche mechanism was first proposed in the 1930s by A. von Hippel and quantum mechanically substantiated by H. Fröhlich [19, 20]. The model of impact ionization of atoms of matter by electrons gives high current densities in the breakdown channel, but does not explain its crystallographic direction and high speed of movement.

In contrast to anodic breakdown, electrical breakdown from the cathode, in particular in alkali hydroxide, is characterized by the absence of crystallographic orientation, subsonic speed of movement and an uneven surface of the breakdown channel [10, 11]. According to the authors of [14], impact ionization and excitation of luminescence centers are observed only in channels of increased electrical conductivity created under the influence of a superstrong electric field. These channels are regions with a modified structure that have a high concentration of linear and point defects.

Previously, it was shown that anodic electrical breakdown in alkali halide crystals [21-27], quartz [28], semiconductor CdS [29], solid [30, 31] and liquid [32] organic substances with long chains of atoms, water [33] is described by the mechanism of interatomic cascade Auger transitions in the valence band of the dielectric. The appearance, movement and orientation of the electrical breakdown channel is determined taking into account data on the crystal chemical and energy structure of the substance.

In this paper, the general principles of the process of formation of an anodic channel of electrical breakdown in various materials are described within the framework of the mechanism of generation of free electrons due to interatomic Auger transitions.

Mechanism of interatomic cascade Auger transitions

Generation of free carriers

Most of the research into the properties of electrical breakdown has been carried out using alkali halide crystals, as materials with well-studied physical properties. The energy band diagram in the region of contact between the metal electrode and the KCl sample in a strong electric field is shown in Fig. 1. The energy levels of the states of K and Cl atoms are given in accordance with the data from [34].

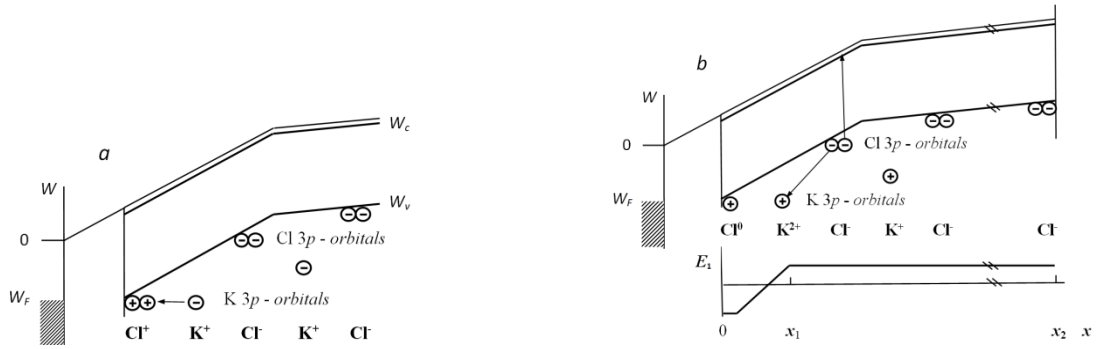

Fig. 1. Scheme of resonant (a) and Auger (b) transitions in KCl in a strong electric field. Wc, Wv, W_F - energy levels of the conduction band bottom, crystal valence band ceiling and the Fermi metal, respectively.

According to [23-25], the beginning of the formation of a breakdown channel is determined by processes at the metal-insulator interface. With an average field strength in the sample of ~10^6 V/cm, the actual field strength near the microtips of the electrode can be more than ~10^8 V/cm. In the near-electrode region of the dielectric, due to the tunneling transition of electrons into the metal, C^+ ions with two holes in the 3*p* orbitals are formed. To do this, a voltage *U* is required such that the edge of the valence band of the dielectric rises to the Fermi level of the metal. It is most likely that the neighboring potassium atom participates in the process of hole recombination through resonant electron transfer from the 3*p* level of potassium to the 3*p* level of chlorine. In the crystal KCl 3*p*, the K^+ level is ~ 6.1 eV below the bottom of the band gap. The process is realized when the energy of the 3p level of potassium in an electric field increases by 6.1 eV (Fig. 1, a). The decay of a hole into K^{2+} occurs as a result of the interatomic Auger transition of an electron from the 3*p* orbital of the neighboring Cl atom and the subsequent generation of an Auger electron into the conduction band (Fig. 1,b). The Auger transition is possible provided that the minimum energy gap between the 3*p* - level K^{++} and the 3*p* - level Cl^- in the electric field is not less than the dielectric band gap *W*g = 7.5 eV.

Issues related to estimating the electric field strength on the surface of the breakdown channel front are considered in [24, 25]. In alkali halide crystals, the necessary band bends for Auger transitions are provided by the electric field of the space charge (SC), which includes a layer of doubly and layers of singly charged halogen ions. The front of the breakdown channel coincides with the boundary of the space charge.

A possible version of the SC fragment is shown in Fig. 2. On the surface of the space charge there are five K^{++} and four Cl^+ ions; deeper layers contain K^+ and Cl^0 ions. The first layer corresponds to the original crystal.

The electric field of the space charge E_s bends the energy zones of the crystal. Electron energy levels drop down as they approach positive space charge. The change in the energy of electronic levels ΔW on the surface of the space charge (transition 1, Fig. 2) can be represented as

$$\Delta W = e(\Phi_K - \Phi_{Cl}), \quad (1)$$

where e is the electron charge, Φ_K, Φ_{Cl} are the potentials in the space occupied by K^{++} and Cl^- ions, respectively.

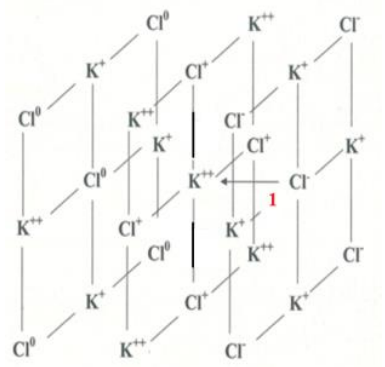

Fig. 2. Fragment of space charge in a KCl crystal.

The main contribution to the change in potential is made by nearby ions. In the potassium chloride lattice of the negative ion in the first environment at a distance $r_1 = a$ (r_1 is the distance from the ion to the nearest spheres of the environment) there are 6 positive ions. In the second environment there are 12 negative ions, for which $r_1 = a\sqrt{2}$ [35].

The value of the potential in the space occupied by the negative Cl^- ion (transition 1, Fig. 2) is determined by the charges of the crystal lattice, the K^{++} ion in the first sphere of the environment and four Cl^+ ions in the second

$$\Phi + \Phi_{Cl} = \frac{e}{4\pi\varepsilon\varepsilon_0 a}\left(\frac{5}{1} + \frac{1\times 2}{1} - \frac{8}{\sqrt{2}} + \frac{4\times 1}{\sqrt{2}}\right), \quad (2)$$

where Φ - is the field potential of the crystal lattice, ε and ε_0 are the dielectric constant of the sample and the electrical constant, respectively. Let's add to the sum in brackets the terms 1/1, - 1/1, and 4/√2, - 4/√2. We get

$$\Phi_{Cl} = \frac{e}{4\pi\varepsilon\varepsilon_0 a}\left(\frac{1}{1} + \frac{4\times 2}{\sqrt{2}}\right). \quad (3)$$

According to (3), the K^{++} ion in the crystal lattice has an effective charge of +1, and the Cl^{+} ion has a charge of +2. Since the Auger transition time $\tau_A \approx 10^{-16}$ - 10^{-17} s [35], then ionic polarization does not occur, and we can assume $\varepsilon \approx \varepsilon_\infty$, where ε_∞- is the optical dielectric constant. As applied to the KCl crystal, a = 3.14 Å, ε_∞ = 2.17 [35]. Value $\Phi_{Cl} \approx 14$ V.

In the space occupied by the K^{++} ion, the value of the potential, taking into account the lattice charges, four Cl^{+} ions and one Cl^{0} in the first sphere and four K^{++} ions in the second, is

$$\Phi + \Phi_K = \frac{e}{4\pi\varepsilon\varepsilon_0 a}\left(-\frac{1}{1} + \frac{4\times 1}{1} - \frac{1\times 0}{1} + \frac{8}{\sqrt{2}} + \frac{4\times 2}{\sqrt{2}}\right). \quad (4)$$

Let's add to the sum in brackets the terms 5/1, -5/1, and $4/\sqrt{2}$, $-4/\sqrt{2}$. We get

$$\Phi_K = \frac{e}{4\pi\varepsilon\varepsilon_0 a}\left(\frac{4\times 2}{1} + \frac{1}{1} + \frac{4\times 1}{\sqrt{2}}\right). \quad (5)$$

The effective charge of the Cl^{0} ion in the lattice is +1. The value is $\Phi_K \approx 24.8$ V. The change in the energy of the electronic levels (1) is $\Delta W \approx 10.8$ eV, which is sufficient to realize the Auger transition.

Crystallographic orientation of breakdown channels

The crystallographic orientation of breakdown channels in alkali halide [21, 23], quartz [28], and single-crystal CdS [29] was determined taking into account data on the crystal chemical and energy structure of the substance.

In ionic-covalent crystals, the upper valence subband is formed by the orbitals of halide ions, and below is the subband formed by the orbitals of metal ions [34, 35]. The energy difference between these W_1 subbands for alkali hydroxide crystals can differ from a few to tens of electron volts [34]. The decay of a hole in the Cl^{+} ion is most preferable from a nearby cation. For a resonant transition of an electron from the cation level, it is necessary to raise it energetically in an electric field to the energy level of the anion. This situation is possible for crystals with W_1 in the energy range 2 - 10 eV. In this case, the orientation of the breakdown channel corresponds to the <100> crystallographic direction. For crystals with energy $W_1 > Wg$, hole recombination will occur from the anion through the Auger transition of the electron in the <110> direction.

The movement of the discharge channel in CdS is associated with the transfer of a positive charge in a straight direction sequentially along the nearest sulfur ions and the generation of Auger electrons into the conduction band of the crystal [29].

Movement of the breakdown channel

The single cycle of the space charge front movement can be divided into three successive stages. At the first stage, when the critical local electric field strength ~ 10^8 V/cm is reached, a resonant transition of the electron from K^{+} to the Cl^{+} atom occurs in a time $\tau_r \sim 10^{-16}$ s and the channel moves to the interatomic distance (Fig. 1, a). The second stage is associated with the recombination of a hole on K^{2+} due to the interatomic Auger transition of an electron from a neighboring chlorine atom during a time $\tau_A \sim 10^{-16}$ s and the generation of an Auger electron into the conduction band of the dielectric. The channel moves one more interatomic distance (Fig. 1, b). The negative charge of electrons reduces the charge field of holes and, accordingly, the bending of bands near the boundary of the charge zone. The third stage is associated with the extraction of electrons by an external electric field from the space charge region, and the achievement of a critical field strength for the next cycle. Cycle time Δt can be represented as

$$\Delta t = \tau_r + \tau_A + \tau_1, \quad (6)$$

where τ_1 - time to reach the critical field strength.

Formation of space charge

The formation of a space charge at the boundary of the conducting layer at $x = x_1$ (Fig. 1) with concentrations of free electrons n and stationary holes p is described by the continuity equations (7) and Poisson equations (8)

$$\frac{\partial \rho}{\partial t} = G - \frac{\partial}{\partial x}\left(en\mu E\right), \quad (7)$$

$$\frac{\partial E}{\partial x} = \frac{\rho}{\varepsilon\varepsilon_0}, \quad (8)$$

where μ is the electron mobility, $\rho = e(p - n)$ is the volume charge density; $E = E_0 + E_1$ is the total electric field strength ($E_0 = U/x_2$, E_1 are the external electric field and space charge strengths, respectively); G - is the volumetric rate of charge generation of Auger electrons in space from x_1 to $x_1 + \Delta x$; where $\Delta x \sim 4$ Å is the thickness of the atomic layer in the crystal. Auger generation switch-on time from t_k to $t_k + \tau_A$, where t_k is the time to reach the critical field strength,

The initial (9) and boundary (10) conditions of the problem will be as follows

$$\text{at } t = 0 \text{ field strength } E = 0, \quad (9)$$

$$\text{for } x \geq x_1 \text{ values } \sigma = 0, \text{ we denote } E_1 = E_s(t), \quad (10)$$

where $E_s(t)$ is the electric field strength beyond the boundary of the space charge x_1, $\sigma = en\mu$ is the conductivity. After transformations (7), (8) we get

$$\varepsilon\varepsilon_0 \frac{\partial^2 E}{\partial x \partial t} = G - \sigma\frac{\partial E}{\partial x}. \quad (11)$$

Integrating (11) over the x coordinate using the boundary condition (10) gives the equation

$$\varepsilon\varepsilon_0 \frac{\partial E}{\partial t} = Gx_1 - \sigma E_0 - \sigma E_1 + \varepsilon\varepsilon_0 \frac{\partial E_s}{\partial t}. \quad (12)$$

The short circuit condition has the form (13)

$$\int_0^{x_2} E_1 dx = 0. \quad (13)$$

To a first approximation, equation (13) can be represented as

$$E_1 x_1 + E_s (x_2 - x_1) = 0. \quad (14)$$

To find E_1 in (12), we express E_s in terms of E_1 and integrate equation (12) along the x coordinate from x=0 to x_2.

$$\varepsilon\varepsilon_0 \int_0^{x_2} \frac{\partial E_1}{\partial t} dx = \int_{x_1}^{x_1+\Delta x} Gx_1 dx - \sigma\int_0^{x_1} E_0 dx - \sigma\int_0^{x_1} E_1 dx - \varepsilon\varepsilon_0 \frac{x_1}{(x_2 - x_1)} \int_0^{x_1} \frac{\partial E_1}{\partial t} dx. \quad (15)$$

Taking into account the short-circuit condition (13), we obtain

$$\frac{\partial E_1}{\partial t}+\frac{E_1}{\tau}=-\frac{E_0}{\tau}+\frac{G\Delta x}{\sigma\tau}, \qquad (16)$$

where $\tau = \varepsilon\varepsilon_0 x_1/\sigma(x_2-x_1)$ is the time constant of the circuit.

The solution to equation (16) with respect to E_1 is found in the form

$$E_1=-E_0\left(1-e^{-\frac{t}{\tau}}\right)+\frac{G\Delta x}{\sigma}\left(1-e^{-\frac{\tau_A}{\tau}}\right). \qquad (17)$$

A decrease in the field strength E_1 of the positive space charge occurs due to the inclusion of the field of Auger electrons. In the absence of Auger generation, the field strength E in the sample region 0 - x_1 is equal to

$$E=E_0\,exp\left(-\frac{t}{\tau}\right). \qquad (18)$$

In the region x_1 - x_2, the field strength E_s of the positive volume charge Q_s, taking into account (14), is determined by the dependence

$$E_s=\frac{E_0 x_1}{\left(x_2-x_1\right)}\left(1-e^{-\frac{t}{\tau}}\right). \qquad (19)$$

In a uniform external field, the intensity E_s increases superlinearly with increasing coordinate x_1 (19). At $x_1 = 0.5x_2$ the value $E_s = E_0$ followed by a sharp increase at $x_1 > 0.7\,x_2$. The spatial structure of the electric field of the space charge E_1 in the 0-x_2 space is presented in Fig. 1. A positive space charge Q_s induces a corresponding charge of a negative sign in the metal electrodes.

To estimate the charge Q_s that creates the intensity E_s, we use the Ostrogradsky–Gauss theorem [36]. Let's construct a closed cylindrical surface with bases: S_1 in the section where E_s vanishes (Fig. 1) and S_2 in the area x_1 - x_2. Since the entire flow of the electric field strength vector leaves the charged region in one direction through the surface S_2, then for a unit surface area of the charged layer, according to the Ostrogradsky-Gauss law, the condition is satisfied

$$\varepsilon\varepsilon_0 E_s=Q_s\left[\frac{k}{cm^2}\right]. \qquad (20)$$

The space charge Q_s is formed in time $t_0 \approx (2\text{-}3)\tau$ and increases with x_1

The spatial charge distribution at the boundary $\sigma = 0$ is close to equilibrium at times comparable to or exceeding τ. Let's imagine $n(x) = n_0 - \Delta n(x)$. The stationary equation for the concentration distribution $\Delta n(x)$, without taking into account the generation of carriers, according to (7) has the form:

$$-\mu\frac{\partial\Delta n}{\partial x}E+\mu(n_0-\Delta n)\frac{\partial E}{\partial x}=0. \qquad (21)$$

At a high electron concentration, we can neglect Δn compared to n_0 in the second term of equation (21), and also take $E \approx E_0 + E_s$. Using the Poisson equation (8), we obtain

$$-\frac{\partial\Delta n}{\partial x}+\frac{\Delta n}{L}=0, \qquad (22)$$

where $L = \tau_m\,\mu\,(E_0 + E_s)$ is the field screening length, $\tau_m = \varepsilon\varepsilon_0/\sigma$ is the Maxwellian relaxation time. We write the boundary condition to equation (22) as $\Delta n(x_1) = n_{s1} = n_0 - n_s$, where ns is the surface electron density at $x=x_1$. The spatial distribution of the electron concentration, taking into account the solution of equation (22), has the form $n(x) = n_0 - n_{s1}\exp(-(x_1 - x)/L)$. The value of $n(x)$ in the $x=x_1$ plane is equal to n_s and exponentially tends to n_0 as the distance x decreases. The distribution of the positive charge density of holes has the form $\rho(x) = e(p - n(x))$.

In the case of a non-uniform field, the maximum intensity near the tip E_m in the "hyperboloid of revolution – plane" electrode structure is equal to [37]

$$E_m=\frac{2U}{r\,ln\frac{4d}{r}}, \qquad (23)$$

where r is the radius of curvature of the electrode, d is the thickness of the sample. The change in the electric field strength E_x as a function of the x coordinate in the 0–x_2 gap of the dielectric can be determined from the expression [37].

$$E_x=\frac{r}{r+x}E_m. \qquad (24)$$

The distribution of E_x is non-uniform and obeys a hyperbolic law. In a non-uniform field in the interval 0 – x_2 there is a point x_{mid}, where $E_x(x_{mid})=E_{mid}$. This means that in the region from the tip electrode to the x_{mid} position the voltage is higher than E_{mid}, and in the region from x_{mid} to the flat electrode it is lower. Value $x_{mid} \approx (0.25\text{-}0.3)x_2$. Field enhancement coefficient at the electrode $\beta = E_m/E_{mid}$.

The electric field at the boundary of the space charge in the structure of the tip-plane electrodes, taking into account the calculations performed, is equal to

$$E_{s1}(t)=E_m\frac{r\,ln\left(\frac{r+x_1}{r}\right)}{\left(x_2-x_1\right)}\left(1-exp-\frac{t}{\tau}\right). \qquad (25)$$

The calculated distribution curves of the external field E_x/E_m and the space charge field E_{s1}/E_m in the 0-x_2 space of the sample at $r \approx 50$ μm are presented in [28]. The charge field strength E_{s1}/E_m increases superlinearly in the region 0-x_2, the value $E_{s1}/E_m = E_x/E_m$ at $x \approx 0.3x_2$.

Pre-breakdown currents

The conduction current density in the space 0 - x_1 is equal to

$$i_1 = \sigma E = \sigma\,E_0 \exp(-t/\tau). \qquad (26)$$

The displacement current density in the space x_1 - x_2 has the form

$$i_s=\frac{\partial Q_s}{\partial t}=\sigma E_0\,exp\left(-\frac{t}{\tau}\right). \qquad (27)$$

The conduction current densities (26) and displacement currents (27) are equal. Equations (26), (27) can also be considered as the dependence of the current density on the position of the space charge $Q_s(x_1)$ in the sample at a time different from t=0. Dependence of the conduction current density function (26) on the argument $t_1 = x_1/v$ (where v is the speed of movement of the breakdown channel, $t_b = x_2/v$ is the breakdown time) at

fixed values of time $t_{01}=0.1\cdot\tau_m$ (curve 1), $t_{02}=0.05\cdot\tau_m$ (curve 2) and $t_{03}=0.01\cdot\tau_m$ (curve 3) are shown in Fig. 3. Current density increases slightly with increasing coordinate x_1.

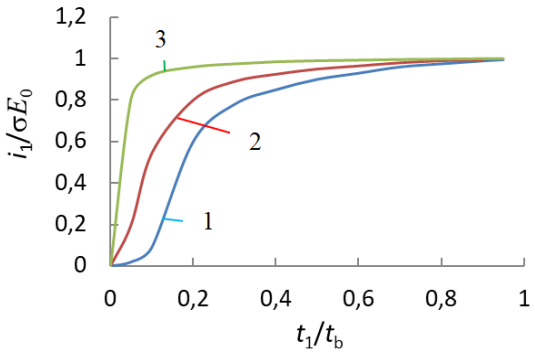

Fig. 3. Dependence of the conduction current density function in the breakdown channel on time

In the experiment, registration of pre-breakdown currents at the front of the voltage pulse is associated with the need to use bridge measurement circuits to compensate for capacitive recharge currents [38, 39].

Oscillograms of voltage U and pre-breakdown current I in a NaCl crystal ~2 mm thick with a positive polarity of the tip electrode are shown in Fig. 4 [38].

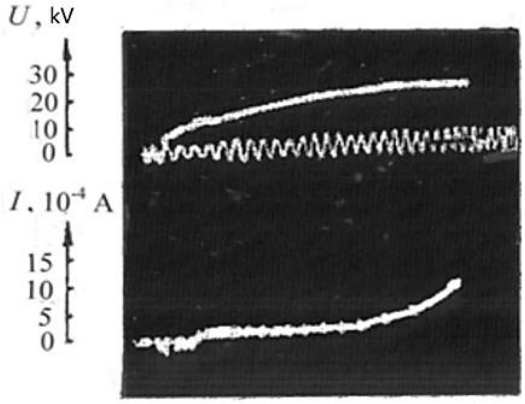

Fig. 4. Oscillograms of a voltage pulse U and current I in a NaCl crystal [38].

The beginning of the discharge propagation is marked on the oscillograms by the appearance of a current of the order of ~10^{-4} A (Fig. 4). As the discharge moves deeper into the sample, the current amplitude remains constant and after 2/3 of the breakdown time it increases exponentially. The maximum current ~10^{-3} A corresponds to the time the channel reaches cathode breakdown. This is followed by a sharp increase in current, which is not reflected in the photograph. According to the data of [38], the diameter of the breakdown channel is expanded at the anode to ~ 2–3 μm and narrows towards the cathode to ~ 0.5–1 μm. The values of the pre-breakdown current for KBr crystals are 2-3 times less than for a NaCl crystal.

It is likely that the destruction of the channel walls is accompanied by the formation of electron-ion plasma, which can increase the strength of the pre-breakdown current.

The dependence of the current strength on time during breakdown in a layer of water 1 cm thick is shown in Fig. 5 [39]. The increase in current near $t \approx 50$ ns corresponds to the beginning of the development of the ionization zone from the tip. At the initial stages of increasing the ionization zone deeper into the gap, the current remains constant (~2 A) until the size of the zone reaches ~5 mm, i.e. approximately half the distance from the tip to the flat electrode. Next, the current increases several times before the ionization zone covers the entire interelectrode gap [39].

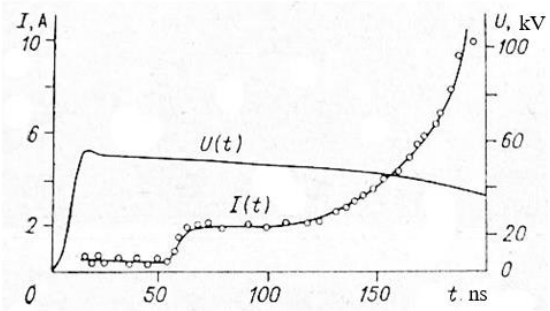

Fig. 5. Pre-breakdown current in water and voltage across the measuring capacitance [39].

In solid and liquid dielectrics, the exponential increase in conduction current at the final stage of breakdown is probably associated with the injection of electrons into the gas phase of the discharge when the walls of the breakdown channel are destroyed and the ionization of the gaseous medium increases.

Breakdown channel movement speed

The time for establishing the critical field strength τ_1 in formula (6) can be determined from the relation

$$\tau_1 = Q_A / i_1 , \quad (28)$$

where $Q_A = \varepsilon\varepsilon_0 \frac{G\Delta x}{\sigma}\left(1 - e^{-\frac{\tau_A}{\tau}}\right)$ is the charge density of Auger electrons in accordance with expression (16). The injection of carriers occurs in a short time and does not depend on the field strength E_0. The cycle time Δt is defined as

$$\Delta t = \tau_r + \tau_A + \frac{G\Delta x \tau_m}{E_0 \sigma} \exp\left(\frac{t_k}{\tau}\right)\left(1 - \exp(-\frac{\tau_A}{\tau})\right) . \quad (29)$$

The formula for Δt allows us to estimate the dependence of the channel speed $v(x_1) \approx \Delta x/\Delta t$ on the coordinate x_1. According to (28, 29), the speed increases with increasing E_0, conductivity σ, coordinate x_1, due to an increase in current i_1.

The experimental picture of the motion of a discharge in a gap of water with a uniform field of ~2 MV/cm is presented in Fig. 6. Time between frames ~1 ns, average speed ~10^7 cm/s. The length of the anode glow increases superlinearly during the development of the channel to the cathode [17].

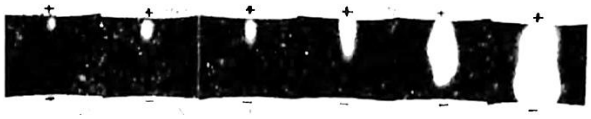

Fig. 6. Change in time of the length and diameter of the anode glow during breakdown in water [17].

The result of the experiment (Fig. 6) is in satisfactory agreement with the calculation data (29), where it is shown that the increase in speed $v(x_1)$ occurs with increasing coordinate x_1.

A cycle of measurements of the speed of movement of the breakdown channel at high electric field strengths in the nanosecond range of breakdown time in samples of alkali halide crystals and liquids was carried out by the authors of [11, 27, 28, 32]. The source of high-voltage nanosecond pulses in the experiment was a pulse generator. Voltage pulses with an amplitude of 60-320 kV with a duration of ~ 8 ns with fronts less than ~ 0.5 ns were generated as a result of the discharge of the coaxial forming line of the generator, charged from a Tesla transformer. The samples were installed between electrodes of the "point-plane" configuration. Voltage pulses of positive polarity were applied to the tip.

Data on the breakdown channel velocity v in samples of KBr, KCl. NaCl, ~1 cm thick, depending on the voltage, was determined by the electron-optical method (Fig. 7) [11].

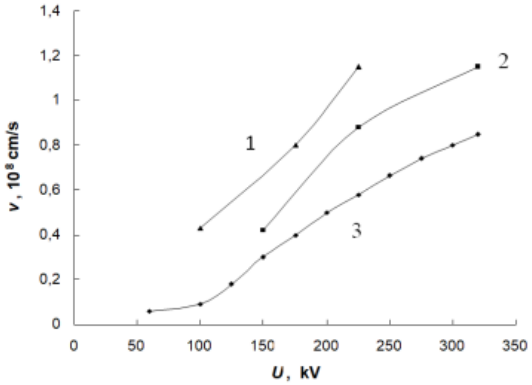

Fig. 7. Dependence of velocity v on voltage U in 1-KBr samples. 2-KCl. 3-NaCl [11]

The speed v increases superlinearly with increasing voltage in the region of 60-140 kV and tends to saturate at voltage values of 150-300 kV (Fig. 7). The value of v decreases in the series of samples of KBr, KCl, NaCl.

Higher field strengths can be obtained in dielectric plates with a thickness d~ 0.5 – 3 mm. The speed of propagation of the breakdown channel was determined by the time interval t_c between the moment the pulse was applied and the moment of a sharp increase in the current through the sample during breakdown [27, 32].

The average velocity v in KCl samples at voltages of 140 and 230 kV was ~$4.5 \cdot 10^7$ and ~$2 \cdot 10^8$ cm/s [27, 40]. The time of movement of the breakdown channel along the path of two interatomic distances for a KCl crystal at a=3.14 Å, the number of ions per 1 cm $\boldsymbol{N}$=$3.2 \cdot 10^{17}$ is equal to Δt = 1cm/($v \cdot 0.5\boldsymbol{N}$) ≈ $1.4 \cdot 10^{-15}$ s and ~ $5.4 \cdot 10^{-16}$ s, respectively.

According to (29), at high levels of conductivity and electric field strength, when E_0 is significantly higher than the dielectric strength E_b, time τ_1 can become comparable to or less than $\tau_r+\tau_A$. In this case, the speed of movement of the boundary of the charge $v(x_1)$ is determined by the time of interatomic transitions and is probably relatively stable with a small change in E_0.

According to the data of [40], the value of v in KCl single crystals at a voltage of 230 kV practically does not change with the thickness of the samples in the range d ~_ 0.6−1.2 mm. In the field of tensions $E \approx E_b$, the parameters of the breakdown channel movement are largely determined by time τ_1. The speed increases with increasing E_0 and σ, which is confirmed experimentally [11, 27, 32].

Breakdown channel resistance

The effect of the sample conductivity level on the breakdown time t_c in KCl, KBr crystals with a thickness of d ~ 0.5 – 3 mm was studied at a voltage of 140 kV [27]. The breakdown time was measured using a needle anode, as well as with a low-power ballast resistor R_b connected to the needle anode circuit.

The average speed of movement of the breakdown channel v in the KCl sample was ~ $4.5 \cdot 10^7$ cm/s. Connecting ballast resistances of 1.2 kΩ and 2.7 kΩ leads to a decrease in the velocity v_d to ~$3.2 \cdot 10^7$ and ~$2.2 \cdot 10^7$ cm/s, respectively. In KBr samples the value of $v \approx 5 \cdot 10^7$ cm/s, the velocity decreased to $v_d \approx 2.4 \cdot 10^7$ cm/s at R_b = 2.7 kΩ connecting the ballast resistor R_b, the total circuit resistance R_z is equal to

$$R_z = R_b + R_0 , \qquad (30)$$

where R_0 is the resistance of the breakdown channel with length x_2. The role of the ballast resistor in calculating the time τ_1 can be taken into account by connecting it to the sample at $x = 0$ in the form of a thin layer of thickness $\Delta x_b << x_2$ with constant conductivity and dielectric constant ε. Resistance R_z can be represented in terms of conductivity σ_z, length x_2 and cross-sectional area of the channel S

$$\frac{x_2}{\sigma_z S} = R_0 \left(\frac{R_b}{R_0} + 1 \right) . \qquad (31)$$

Time Δt for $x_1 > \Delta x_b$ can be written as

$$\Delta t = \tau_r + \tau_A + \frac{G \Delta x \varepsilon \varepsilon_0}{E_0 \sigma_z^2} \exp\left(\frac{t_k}{\tau} \right) \left(1 - \exp\left(-\frac{\tau_A}{\tau} \right) \right) . \qquad (32)$$

According to (32), the cycle duration is related to conductivity by an inverse quadratic dependence, which gives increased sensitivity of Δt to changes in conductivity.

Since at a voltage of 140 kV the time $\Delta t \approx 1.4 \cdot 10^{-15}$ s, then in (32) the values of τ_r and τ_A can be neglected in comparison with the time τ_1. In this case, the ratio of breakdown rates with and without ballast resistance, taking into account (32) and (29) takes the form

$$\frac{v_b}{v} \approx \left(\frac{\sigma_z}{\sigma} \right)^2 . \qquad (33)$$

Passing from conductivity σ and σ_z to resistances R_0 and R_z, equation (33) will be written

$$\frac{v_b}{v} \approx \frac{1}{\left(R_b / R_0 + 1 \right)^2} . \qquad (34)$$

Calculation of the channel resistance in KCl and KBr samples using formula (34) was reduced to determining the value of R_b/R_0 and then R_0.

The work revealed inhomogeneity of the resistance of the breakdown channel depending on the length of the sample. The resistance increases almost linearly with channel length for thin KCl, KBr samples with a thickness of 0.5 – 0.8 mm. In the range of 0.8 – 1.1 mm it goes through a saturation stage, and then remains constant up to the maximum measured thickness of 2.5 – 3 mm. Analysis of the dependence $R_0(d)$ suggests that the head region with a length of ~1 mm has the greatest resistance. [27].

The average channel resistance for samples with a thickness of 2.5–3 mm in KCl is $R_0 \approx 6.5$ kΩ and in KBr ~ 6.1 kΩ.

Breakdown channel structure

The internal structure of the electrical breakdown channel includes the regions of the gas phase, the transition solid layer, and the space charge at the boundary σ = 0 [27].

The specific conductivity of the gas medium of the channel with its diameter ~ 10 μm [11], length 1 mm, resistance in KCl $R_0 \approx 6.5$ kΩ is $\sigma \approx 20$ $\Omega^{-1}cm^{-1}$ and in KBr at $R_0 \approx 6.1$ kΩ is $\sigma \approx 21$ $\Omega^{-1}cm^{-1}$. The higher conductivity in KBr compared to KCl satisfactorily correlates with the higher speed of the breakdown channel according to equation (29). Taking into account the experimental density of the prebreakdown current ~10^4-10^5 A/cm^2 [38, 39], in a time of ~10^{-9} s a Joule energy of ~$5 \cdot 10^{-1}$ J/cm^3 is released per unit volume of KCl, which is significantly less than the heat of fusion ~ 0.68 kJ/cm^3.

A temperature close to the melting point is provided by the mechanism of recombination heat release due to a decrease in the initial carrier concentration, which is probably $n_1 \sim 10^{21}$ cm^{-3} near the boundary σ = 0 [25]. Nonradiative recombination of electrons and holes leads to the release of heat and an increase in thermal pressure P_T due to the vibration of atoms around the equilibrium position. The heat of recombination per unit volume can be estimated as $W_T = (n_1 - n)W_g$. The relationship between thermal pressure and thermal energy per unit volume is given by the equation

$$P_T = \gamma W_T , \qquad (35)$$

where γ is the Grüneisen coefficient [42].

An increase in thermal pressure is accompanied by an expansion of the heated volume. The movement of the substance proceeds sequentially from the surface boundary to the axis of the breakdown channel at the speed of sound v_s. In KCl samples, with a breakdown channel diameter $d_k \sim 1$ μm, sound speed $v_s \sim 4.52 \cdot 10^5$ cm/s [35]. Acoustic relaxation time $\tau_a = (0.5 d_k)/v_s \approx 10^{-10}$ s. During time τ_a, the electron concentration near x_1 drops according to [25] to $n_2 \approx 10^{16}$ cm^{-3}. The energy released per unit volume is $(n_1 - n_2)Wg \approx 1.4$ kJ/cm^3, which is comparable to the heat of fusion for KCl ~ 0.68 kJ/cm^3, but less than the heat of evaporation 5.5 kJ/cm^3 [10, 11]. The pressure near the boundary $(x_1 - x) \approx 10^{-3}$ cm, according to (35), is ~ 10^9 Pa. This pressure corresponds to weak shock waves and is capable of deforming the material adjacent to the channel walls.

It is likely that the transitional heated region is in the solid state, since with such compressions, the transition to the liquid state requires a heat of fusion that is 1.5–2 times greater than the heat at atmospheric pressure [42]. This is due to the fact that when a substance is compressed, the height of the potential barrier increases, which an ion must overcome in order to leave

its site of the crystal lattice. Considering that the tensile strength of alkali halide crystals does not exceed ~ $5 \cdot 10^6$ Pa [10], deformations in the heated region along the channel axis, in the direction of the positive electrode, will lead to destruction of the substance and the formation of a gas phase.

The length of the transition region from the solid to the gas phase was estimated as the product of the time of destruction of the material under the action of elastic stresses and the speed of movement of the breakdown channel. The length of the transition region of the channel at velocities $v \sim 10^7 - 10^8$ cm/s is $\tau_a \cdot v \sim 10 -$ 100 μm. The result of estimating the size of the transition region (tens of microns) is in agreement with the data of [10, 11], where it was shown that the glow in the breakdown channel is associated with a discharge in the gas phase, and the length of the glow and the length of the channel have similar values.

It should be noted that the inhomogeneity of the gas medium resistance along the breakdown channel [27] reflects the time process of its formation in terms of composition and ionization level. Probably, the head region of the gas phase with increased resistance includes crystal microparticles. Under the influence of temperature, clusters disintegrate into metal and halogen ions. The lifetime of such clusters can be determined as ~ 100 μm/$4.5 \cdot 10^7$ cm·s^{-1} ≈ $2.2 \cdot 10^{-9}$ s.

The high resistance of the head part of the gas phase of the breakdown channel is consistent with the data from a study of the energy and mass composition of the plasma, confirming the low level of content of multiply charged ions in the primary breakdown channel of KCl samples [41].

In the general case, the effect of hole self-localization removes the requirement for equality of particle momenta during recombination in alkali-halide crystals, and impact recombination with heat release occurs at a carrier concentration of ~10^{16} cm^{-3} [25]. In a CdS crystal, quadratic recombination with light emission and weak manifestation of impact recombination do not provide the necessary thermal pressure for destruction in the streamer channel [30].

The spatial structure of the breakdown channel is formed by a set of single Auger transition channels (Fig. 1) and includes a positive space charge and a conducting channel of complex phase composition with electron-hole plasma. The channel front moves from the positive electrode into the sample. The channel diameter is probably determined by the size of the area in the near-surface region of the dielectric, within which a layer of C^+ ions is formed. Its size is proportional to the external voltage. This pattern was previously observed for KCl samples, in which the diameter of the breakdown channel increased from 8 to 24 μm with a voltage in the range of 150–315 kV [11].

Radial stability of the electrical breakdown channel

It should be noted the high stability of the transverse dimensions of the breakdown channel in alkali halide crystals over a fairly large length (Fig. 8)

Fig. 8. Channel of incomplete pulsed anodic breakdown in crystalline KCl (sample thickness 1.5 mm)

The fact of radial stability of the channel is possible with a flat front boundary and the same speed of movement of sections of the surface of the orbit. To do this, it is necessary that the time to reach the critical field strength τ_1 in the space charge region maintains a fixed value along the entire front. According to (29), the current density $E_0\sigma$ in the cross section of the channel should have a constant value. At the periphery of the SC region, due to Auger electrons escaping from the channel, the conductivity becomes lower than in the center. However, in alternating and pulsed electric fields the skin effect operates, leading to an increase in the electric field strength on the surface of the conducting channel. Probably, the antibatal nature of the change in E_0 and $\sigma 0$ in the cross section of the channel contributes to the condition $E_0\sigma \sim$ const in the plane of the front of the SC and, accordingly, to the radial stability of the channel. The manifestation of radial stability of the discharge can be considered a characteristic feature of breakdown channels in alkali halide crystals, quartz, CdS, [29].

Electrical strength of dielectric materials

The electrical strength of a sample is one of the main parameters of electrical breakdown. In this breakdown mechanism, this is the external field strength that ensures the formation of a layer of doubly ionized halogen ions on the surface of the dielectric. [23-25].

In the energy diagram of a metal-dielectric contact, the energy of a stationary electron in a vacuum is taken as the zero level (Fig. 1). The Fermi level of the metal W_F is located below the depth of the electron work function in vacuum W_a. The W_a values for such metals as Al, Fe, Cu are 4.25, 4.31, 4.4 eV, respectively. The bottom of the conduction band of the dielectric is located below the zero level to the depth of the crystal's electron affinity χ. The work function of an electron leaving a dielectric is $\varphi = \chi + W_g$. To carry out a tunneling transition of an electron from an insulator to a metal, it is necessary that the middle of the upper valence subband be raised by the electric field at least to the Fermi level in the metal (the beginning of the zone of free levels for electrons in the metal). In this case, a potential barrier (close to a triangular shape) is formed with a height of ~ □ and an effective width of

~□□/$e \cdot \beta \cdot E$. The probability of electron tunneling through a potential barrier increases sharply as the barrier area decreases above the level of electron transition from the valence band. This occurs when the field strength E increases or when the electron energy in the band gap of the crystal increases (for example, when an electron tunnels from dislocation levels).

To estimate the probability of tunneling of an electron P per unit time through a potential barrier of a triangular shape in a field of strength βE , you can use the dependence [9]

$$P \cong \frac{eEa}{h} \exp\left(-\frac{\pi^2 ma\varphi^2}{eh^2 \beta E}\right), \qquad (36)$$

where a is the distance between unlike ions in the lattice, h is Planck's constant. For a dielectric with a ~ 3 Å and Wg ~ 10 eV in a field $\beta E \sim 2 \cdot 10^8$ V/cm with a process duration Δt_1 comparable to the lifetime of the ionized state of a halogen atom ~ 10^{-14} s, we obtain the tunneling probability $P_1 \, \Delta \, t_1 \approx 0.2$.

The dependence of the electrical strength E_b for various alkali halide crystals on the work function □ is shown in Fig. 9. Values E_b were obtained in quasi-static mode (data 1), with a field application duration of 30 ns (data 2) and ~10 ns (data 3) [9, 10, 23]. It was taken into account that in experiments measuring E_b, the electric field was applied to the crystal in the <100> direction. In KBr and KCl crystals, the breakdown channels are oriented in the <100> direction. In crystals of NaCl, NaF, LiF along <110>. In this case, the field strength in the <110> direction will be less than Eb by a factor of 1.41 compared to the <100> direction. This is confirmed by the results of [10], according to which for NaCl crystal plates cut with the transverse direction <110> and <100>, the breakdown voltage ratio was ~ 1/1.41. Arrows in Fig.9 a decrease in breakdown strength by 1.41 times is shown for a NaCl, NaF, LiF crystal.

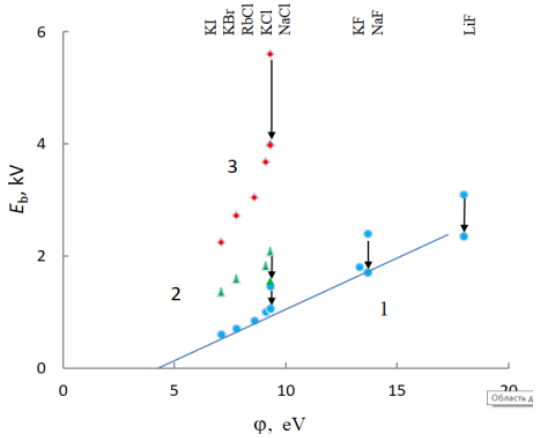

Fig. 9. Dependence of electrical strength E_b on the value of φ for various dielectrics. 1-data of the quasi-static mode [9], 2-with a field pulse duration of 30 ns (sample thickness ~ 0.15 mm) [10], 3-experimental results [23]

The effect of an increase in breakdown voltage with a decrease in the duration of the field pulse is probably associated with the presence of surface energy levels in the band gap of the crystal, formed by the emergence of point and linear defects on the surface [14]. Shortening the field duration reduces the concentration of newly created defects and their movement towards the surface. Accordingly, the number of valence band electrons tunneling through defect levels decreases, which leads to an increase in the electrical strength of the sample.

The values of the electrical strength of crystals in the quasi-static measurement mode increase almost linearly with increasing φ (Fig. 8). The trend line cuts off a segment equal to ~ 4.5 eV on the ordinate axis, which is comparable to the value of W_a. Such a linear relationship can be described by an equation of the form

$$E_b \, \beta \, \Delta x \, e = - W_a + \varphi, \qquad (37)$$

where the left side of the equation is the change in electron energy near the electrode at an interatomic distance of the order of $\Delta x_1 \approx 1-2$ Å at electric field strength $E_b\beta$. Equation (37) reflects the situation of raising the edge of the valence band of the dielectric to the Fermi level of the metal (Fig. 1).

Thus, a necessary and sufficient condition for the formation of a layer of doubly ionized halogen ions on the surface of the dielectric is the transition of electrons from the valence band of the dielectric to the free energy levels of the metal.

Conclusion

The mechanism of electron generation into the conduction band of a dielectric through interatomic cascade Auger transitions in the valence band opens up new opportunities for understanding the process of electrical breakdown and its control.

It is possible to make a qualitative and quantitative interpretation of a number of basic properties of electrical breakdown and the process of its formation within the framework of this mechanism. In particular: the crystallographic orientation of the breakdown channels, taking into account the electronic structure of the valence band of the dielectric; high density of pre-breakdown current (~10^4 A/cm^2) without involving the effect of impact ionization of atoms of a substance by free electrons of the conduction band; high breakdown speed ~ 10^8 cm/s, due to the short Auger transition time,

high breakdown voltage and significant electronic conductivity.

It has been shown that heating and high pressure in the transition layer are caused by the release of heat during nonradiative recombination of electrons and holes; the internal structure of the electrical breakdown channel includes the regions of the gas phase, transition solid layer and space charge; the process of electron tunneling transitions forms a layer of doubly positively charged ions of the substance on the surface of the dielectric at a voltage E_b.

An adequate description of the breakdown process allows for a targeted selection of dielectrics and their properties that provide the necessary technical requirements for the electrical insulation of high-voltage devices and installations.

At the same time, in the process of developing model representations of breakdown, a number of problems were identified, the solution of which depends on the improvement and correct description of the electric discharge mechanisms themselves. Experimental and theoretical studies of the process of electron tunneling from the near-electrode region of a dielectric into a metal are of interest. The concentration of carriers at the moment of generation of Auger electrons and the physical nature of the state of matter in the transition region between the gas phase and the solid dielectric remain unclear.

Research into electrical breakdown has been carried out for more than a hundred years, and is very relevant due to its great practical importance and the complexity of physical processes.

References:

1. Monzel W. J., Hoff B. W., Maestas S. S., French D. M., Hayden S. C. Dielectric Breakdown of Additively Manufactured Polymeric Materials. IEEE Tr. Dielectr. Electr. Insul. 2015. V. 22. № 6. pp. 3543-3549. DOI: 10.1109/TDEI.2015.005199 .

2. Dabbak S. Z. A., Illias H. A., Ang B. C., Latiff N. A. A. and Makmud M. Z. H. Electrical Properties of Polyethylene/Polypropylene Compounds for High-Voltage Insulation. Energies. 2018. V. 11. p. 1448. DOI:10.3390/en11061448.

3. Hattori Y., Taniguchi T., Watanabe K. and Nagashio K. Anisotropic Dielectric Breakdown Strength of Single Crystal Hexagonal Boron Nitride. ACS Applied Materials & Interfaces. 2016. 8 (41), 27877-27884.

4. Chen G. and Zuber M. H. Pre-breakdown Characteristics of Contaminated Power Transformer Oil. Annual Report – Conf. on Electr, Insulat. and Diel. Phenomena Vancouver, BC, Canada 14-17 Oct. 2007. DOI:10.1109/CEIDP11960.2007.

5. Bin C., Ji-Wei D., Ming-He C. Electrical Breakdown Mechanism of Transformer Oil with Water Impurity: Molecular Dynamics Simulations and First-Principles Calculations. Crystals. 2021. V. *11*. № 2. p. 123. DOI: 10.3390/cryst11020123.

6. Obidin A.Z., Pechenov A.N., Popov Yu. M., et. al. Spatial-Temporal and Power Characteristics of the Streamer Semiconductor CdS Laser. Kvant. Elektron. 1982. V.9. №8. pp. 1530- 1535.

7. Obidin A.Z., Pechenov A.N., Popov Yu.M., et. al. A Study of Light Generation in the Direction of the Streamer Channel in A^2B^6 Semiconductors. Kvant. Elektron. 1983. V.10. № 6, pp. 1165- 1170.

8. Arbuzov A. I., Bystritskiy V. I., Krasik Ya. E., Lopatin V. S., Usov Yu. P., Tolmacheva V. G., Chistyakov S. A. Sil'notochnyy uskoritel' s vodyanym nakopitelem. Trudy 6 vsesoyuznogo soveshchaniya po uskoritelyam zaryazhennykh chastits. Dubna. 1978. 11-13 oktyabrya. s. 75. (in Russian).

9. Skanavi G. I., Physics of Insulators (Strong Field Range). (Fizmatgiz, Moscow, 1958) (in Russian).

10. Vorobyov A.A., Vorobyov G.A. Electricheskiy proboi i razrushenie tverdykh tel (Izda-vo Vysshaya shkola, M., 1966), 224 s. (in Russian).

11. Vershinin Yu. N. Elektronno-teplovye i detonatsionnye protsessy pri elektricheskom proboe tverdykh dielektrikov (Izda-vo UrO RAN, Ekaterinburg, 2000), 260 s. (in Russian).

12. Mesyats G.A., Pegel' I.V. Vvedenie v nanosekundnuyu impulsnuyu energetiku i elektroniku (FIAN, M., 2009), 192 s. (in Russian).

13. Vorobyov G.A. Effect of Discharge Incorporation into a Solid Insulator Immersed in an Insulating Fluid. Tech. phys. 2005. V. 50. №4. p. 517. DOI:10.1134/1.1901785.

14. Vorobyov G. A., Ekhanin S. G. and Nesmelov N. S. Electrical breakdown of solid dielectrics. Phys. Solid State. 2005. V. 47. № 6. pp. 1083-1087. DOI:10.1134/1.1946860.

15. Kao K. C. New theory of electrical discharge and breakdown in low-mobility condensed insulators. J. Appl. Phys. 1984. V. 55. № 3. p. 752.

16. Mohan Rao U., Fofana I., Beroual A., Rozga P., Pompili M., Calcara L., Rapp K.J. A Review on Pre-breakdown phenomena in Ester Fluids. IEEE Tr. Dielectr. Electr. Insul. 2020. V. 27. № 5. pp. 1546-1560. DOI:10.1109/TDEI.2020.008765.

17. Ushakov V.Ya. Impul'snyy elektricheskiy proboy zhidkostey. (Izda-vo Tomsk St. Univ., Tomsk, 1975). 258 s. (in Russian).

18. Ushakov V. Ya., Klimkin V.F., Korobeinikov S.M., Lopatin V.V. Proboi zhidkostei pri impulsnom napryazhenii (Izd-vo nauch.-tekh. lit-ry,Tomsk, 2005),488 s. (in Russian).

19. Von Hippel, A. Electric Breakdown of Solid and Liquid Insulators. J. Appl. Phys. 1937. V. 8. pp. 815-832.

20. Froehlich, H. Theory of Electrical Breakdown in Ionic Crystals. Proc. R. Soc. London, Ser. A. 1937. 160. pp. 230-241.

21. Kulikov V. D. The mechanism of the streamer stage of breakdown in crystal dielectrics. Tech. Phys. Lett. 2000. V. 26. № 2. pp. 170-172. DOI: 10.1134/1.1262781.

22. Kulikov V. D. Charge Carrier Generation in a KBr Crystal under the Action of a Pulsed Sub-Breakdown Electric Field. Tech. Phys. Lett. 2002. V. 28. № 2. pp. 99-101. DOI: 10.1134/1.1458502.

23. Kulikov V. D. Electrical Breakdown in Ionic Crystals Exposed to Nanosecond Pulses. Tech. Phys. 2003. V. 48. № 12. pp. 1527-1531. DOI: 10.1134/1.1634672..

24. Kulikov V. D. Electrical Breakdown in Ionic Crystals. Tech. Phys. 2009. V. 54. № 1. pp. 56-61. DOI:10.1134/S1063784209010083.

25. Kulikov V. D. Model of the Electrical Breakdown Channel in Ionic Crystals. Tech. Phys. 2012. V. 57. № 2. pp. 192-197. DOI:10.1134/S1063784212020144.

26. Kulikov V. D. Electrical Breakdown in Ionic Crystals (Izda-vo Tomsk St. Univ. Tomsk, 2014). (in Russian).

27. Punanov I.F., Emlin R. V., Kulikov V. D. and Cholakh S.O. Resistance of a Pulsed Electrical Breakdown Channel in Ionic Crystals. Tech. Phys. 2014. V. 59. № 4. pp. 503-507. DOI: 10.1134/S1063784214040197.

28. Emlin R. V., Barakhvostov S. V., Kulikov V. D. Anisotropy of Electrical Breakdown in Crystalline Quartz. Tech. Phys. 2009. V. 54. № 7. pp. 1076-1079. DOI:10.1134/S1063784209070275.

29. Kulikov V., Yakovlev V., Bobkova L. Model of a streamer discharge channel in monocrystalline CdS. NJDIS. 2020. № 44-1. pp. 21-24.

30. Kulikov V. Electrical breakdown of polymeric materials. NJDIS. 2021. № 62-1. pp. 51-54. DOI:10.24412/3453-9875-2021-62-1-51-54.

31. Kulikov V. Barrier effect in dielectric materials. NJDIS. 2023. № 103. pp. 47-52. doi. org/10.5281/zenodo.7688048.

32. Emlin R.V., Punanov I.F., Kulikov V.D. Electronic mechanism of propagation of nanosecond breakdown channel in liquid organic dielectrics. Tech. Phys. 2022. V. 92. № 10. pp. 1342-1348. DOI: 10.21883/TP.2022.10.54361.93-22.

33. Kulikov V. Electric Breakdown in Water. NJDIS. 2023. № 118. pp. 50-54. doi. org/10.5281/zenodo.10009518.

34. Nemoshkalenko V. V and Aleshin V. G. Electron Spectroscopy of Crystals (Naukova Dumka, Kiev, 1976; Plenum, New York, 1979).

35. Wert C. A. and Thomson R. M. Physics of Solids, 2nd ed. (McGraw-Hill, New York, 1970).

36. Tamm I.E. Osnovy teorii elektrichestva. (Nauka, M., 1976). 615 s. (in Russian).

37. Meek J.M., Craggs J.D. Electrical Breakdown of Gases. (Oxford: Clarendon Press, 1953), 507 p.

38. Torbin N. M. Pre-breakdown currents in large thicknesses of solid dielectrics. Izv. Vuzov. Energetika. 1960. № 10. pp. 26–31. (in Russian).

39. Ovchinnikov I.T., Yanshin E.V. Izmereniye predproboynoy elektroprovodnosti vody s pomoshch'yu impul'snogo vysokovol'tnogo elektrooptycheskogo mosta. V kn. Impul'snyy razryad v dielektrikakh. (Izda-vo Nauka, Novosibirsk, 1985), s. 83-88. (in Russian).

40. Emlin R.V., Vershinin Yu.N., Beloglazov V.A. Zavisimost' skorosti formirovaniya kanala vysokovol'tnogo proboya ot napryazheniya v diapazone 110-230 kV v monokristallicheskom KCl. Tr. IX Simposiuma po silnotochnoy elektronike. Nikolaev 21−30 iyulya 1992. (Nauch.-tekh. Redaktsiya Giperoks“, M., 1992), s. 299. (in Russian).

41. Barakhvostov S. V., Muzyukin I. L. Plasma parameters during nanosecond breakdown and capillary discharge in a solid dielectric. Tech. Phys. 2009. V. 54, № 5 pp. 631-634. DOI:10.1134/S1063784209050041.

42. Zel’dovich Ya. B. and Raizer Yu. P. Physics of Shock Waves and High Temperature Hydrodynamic Phenomena (Nauka, Moscow, 1966; Academic, New York, 1967).